

## Chapter 3

### Numerical techniques for solving the coupled Schrödinger equations

Solving coupled linear differential equations like Eq. 2.3 is a problem found in all branches of physics and as such, extensive literature exists on the subject. In most cases one must resort to numerical techniques to solve these equations. Many different numerical methods have been developed over the years and can be broadly divided into two categories, explicit (sometimes called “propagators”) and implicit approaches. Both approaches divide the domain of the independent variable into grids or sectors. Explicit methods require the solution of the dependent variable at the preceding grid point to determine its value at the next adjacent point. Implicit methods typically require the solution of a large set of linear equations (or an eigen-system) and thereby determine the value at all grid points simultaneously. Explicit approaches generally are easy to code, fast, and not memory limited since the solutions are calculated “on the fly”. The Numerov[58], Gordon[59], and log derivative propagator[60] methods are examples commonly used in atomic collision physics; a performance review of these algorithms is given in Ref.[61]. However, implicit methods are inherently more stable[62] and often give better accuracy. Extremely good linear algebra packages (e.g., LAPACK[63]) are now commonly available (and free!). These packages are cpu-efficient and vastly reduce the programming complexity associated with the linear algebra steps. In addition, with recent advances in computer technology, memory is not the prohibitive factor it once was.

In this chapter, I present an implicit method to solve the coupled-channel Schrödinger equations. Section 3.1 develops the basic method which is based on a finite-element (FEM)  $\underline{R}$ -matrix approach. Section 3.2 connects the  $\underline{R}$ -matrix to the physical observables given in terms of a scattering  $\underline{S}$ -matrix. Section 3.3 develops an alternative adiabatic representation to describe the coupled equations. This is presented mainly as a qualitative tool for understanding two-body collisions. However, the power of the adiabatic FEM  $\underline{R}$ -matrix approach is brought to bear to solve the three-body collision equations presented in Chapter 8.

### 3.1 Finite element R-matrix approach

The R-matrix method first introduced by Wigner and Eisenbud[64, 65, 66] (1947) has been extended considerably over the years. The variant presented in Section 3.1.1 is the noniterative eigenchannel R-matrix[67, 68, 23] which is based on the familiar Rayleigh-Ritz variational expression for energy eigenvalues. This is a technique which provides a variational solution for the log derivative of a wave function on a given boundary. The R-matrix method has been used extensively in photoionization studies which are sometimes dubbed “half-collision” processes. Section 3.1.2 describes the finite element basis (FEM) used to solve the R-matrix equations. The use of finite elements to solve differential equations in atomic physics is relatively new[69, 70]. This is one of the first implementations of a FEM R-matrix approach (see also Ref.[71]), although a similiar approach using basis splines (B-splines) has been presented elsewhere[72]. The last section 3.1.3 describes a technique to match R-matrix box solutions to the expected long-range form of the coupled channel solutions. This is useful if a prohibitively large number of channels or sectors are needed to describe the collision complex, such that computer memory becomes short. In this event, the problem can be side-stepped by dividing the radial domain into several boxes and solving the equations in each box separately. An appropriate transformation equates the asymptotic R-matrix with the individual box solutions.

#### 3.1.1 R-matrix equations

The eigenchannel R-matrix method solves the coupled Schrödinger equations (i.e., Eq. 2.3) within a finite reaction volume  $\Omega$  of configuration space, subject to **constant** normal logarithmic derivative boundary conditions on the surface  $\Sigma$  of  $\Omega$ . The collisional properties of the system, typically represented in terms of an S-matrix, are easily obtained by a straightforward matching procedure once the normal logarithmic derivative  $b = -(\partial\Psi/dn)\Psi^{-1}$  is calculated. The present implementation restricts the discussion to a single coordinate  $R$  which represents the internuclear separation. However, the techniques presented here are readily generalized to 2- or 3- dimensions[71].

Rearranging the Rayleigh-Ritz expression, one can obtain the following variational expression for the normal logarithmic derivative  $b$  of the solutions  $\Psi$  of Eq. 2.3 on the surface  $\Sigma$ [67]:

$$b = \frac{\int_{\Omega} 2\mu\Psi^*(E - H)\Psi dw - \int_{\Sigma} \Psi^* \frac{\partial\Psi}{\partial n} dS}{\int_{\Sigma} \Psi^* \Psi dS}. \quad (3.1)$$

Here  $E$  represents the relative collision energy,  $\mu$  the reduced mass, and  $H$  the Hamiltonian of the colliding pair. A typical approach for solving the above equation is to approximate  $\Psi$  using a basis set expansion. A multi-component wave function

can be represented by  $\Psi = \sum_m F_m(R)Y_m(\Omega)\chi_m$ , which upon introducing a basis set expansion for the radial wave function becomes

$$\Psi = \sum_{i'} c_{i'} \phi_{i'}(R)Y_{i'}(\Omega)\chi_{i'} . \quad (3.2)$$

Here,  $Y(\Omega)$  represents a spherical harmonic,  $\chi$  the spin degrees of freedom,  $m$  is an index containing all quantum numbers needed to uniquely define a channel, and  $i'$  incorporates the basis function index with  $m$ . Arbitrary basis functions are designated by  $\phi_{i'}$ , and the coefficients  $c_{i'}$  are to be determined numerically. Insertion of this expansion (Eq. 3.2) into Eq. 3.1, leads to the following generalized eigenvalue equation

$$\underline{\Gamma}\vec{c} = b\underline{\Lambda}\vec{c} . \quad (3.3)$$

The matrix elements of  $\Gamma$  and  $\Lambda$  will be described in the following subsection. In general, Eq. 3.3 can be solved directly obtaining the log derivatives and eigenvectors needed to describe the solution on the boundary  $\Sigma$ . However in practice, the matrices in Eq. 3.3 are quite large and direct diagonalization is inefficient. It has been shown[67] that partitioning the matrices according to whether the basis functions are non-zero (open  $\equiv o$ ) or zero (closed  $\equiv c$ ) on  $\Sigma$

$$\begin{pmatrix} \underline{\Gamma}^{cc} & \underline{\Gamma}^{co} \\ \underline{\Gamma}^{oc} & \underline{\Gamma}^{oo} \end{pmatrix} \begin{pmatrix} c^c \\ c^o \end{pmatrix} = b \begin{pmatrix} 0 & 0 \\ 0 & \underline{\Lambda}^{oo} \end{pmatrix} \begin{pmatrix} c^c \\ c^o \end{pmatrix} \quad (3.4)$$

Eq. 3.3 can be reduced to a small ( $m_P \times m_P$ ) eigensystem

$$\underline{\Omega}^{oo} c^{\vec{o}} = b \underline{\Lambda}^{oo} c^{\vec{o}} \quad (3.5)$$

where  $\underline{\Omega}^{oo} = \underline{\Gamma}^{oo} - \underline{\Gamma}^{oc}(\underline{\Gamma}^{cc})^{-1}\underline{\Gamma}^{co}$ . The main computational burden is thus shifted to solving a set of linear equations

$$\underline{\Gamma}^{cc} \underline{X}^{co} = \underline{\Gamma}^{co} \quad (3.6)$$

whose solution  $\underline{X}^{co} = (\underline{\Gamma}^{cc})^{-1}\underline{\Gamma}^{co}$  provides the needed matrix inverse, after which Eq. 3.5 can be solved efficiently.

### 3.1.2 Finite element basis

The  $\underline{R}$ -matrix equations 3.5 and 3.6 were derived using an arbitrary radial basis expansion. A particularly flexible choice is the FEM basis[73, 74, 69]. The FEM method divides the radial domain into  $n_{\max}$  sectors (or elements) and within each sector defines a **local** basis. The six local basis functions  $u_k(x_n)$  are fifth order Hermite interpolating polynomials which are non-zero only in sector  $n$ . Here,  $x_n$

is a rescaled variable defined on the interval  $[-1,1]$  which is related to the physical internuclear separation  $R$  through the transformation  $R = a_n x_n + d_n$  with sector coefficients  $a_n = (R_{n+1} - R_n)/2$  and  $d_n = (R_{n+1} + R_n)/2$ . The FEM expansion for the radial wave function becomes

$$F(R) = \sum_{i \equiv \{k,m,n\}} c_i u_i(x_n), \quad (3.7)$$

where the set  $i$  contains the basis function index  $k$ , the channel index  $m$ , and the sector index  $n$ . The six basis functions are defined through the following boundary conditions (exact expressions are given in Appendix A):

$$\begin{aligned} u_k(-1) &= \delta_{1k} & u_k(0) &= \delta_{3k} & u_k(1) &= \delta_{5k} \\ \frac{du_k(-1)}{dx} &= \delta_{2k} & \frac{du_k(0)}{dx} &= \delta_{4k} & \frac{du_k(1)}{dx} &= \delta_{6k}. \end{aligned} \quad (3.8)$$

The requirement that each channel component and its first derivative must be continuous across sector boundaries imposes the following constraints on the basis function coefficients  $c_{k,m,n}$

$$c_{5,m,n} = c_{1,m,n+1} \quad c_{6,m,n} = \frac{a_n}{a_{n+1}} c_{2,m,n+1}. \quad (3.9)$$

In addition, channel boundary conditions can be imposed quite simply by setting the value of the appropriate coefficient. For example, the large  $R$  boundary condition in closed channels can be applied at the outset by simply setting  $c_{5,m,n_{max}} = 0$ . This eliminates problems with exponential growth in these channels and, if  $R_{n_{max}}$  is chosen well into the classically forbidden region, there is no loss of accuracy.

The matrix elements of  $\Gamma$  and  $\Lambda$  in the finite element representation are given by

$$\Gamma_{ij} = 2\mu \int_{-1}^1 u_i(x_n)(E - H)u_j(x_n)a_n dx_n - \delta_{m,m'} \delta_{n,n_{max}} \delta_{k,5} \delta_{k',6} / a_n \quad (3.10)$$

$$\Lambda_{ij} = \delta_{m,m'} \delta_{n,n_{max}} \delta_{k,5} \delta_{k',5} \quad (3.11)$$

where  $i \equiv \{k, m, n\}$  and  $j \equiv \{k', m', n\}$ .  $H$  is the Hamiltonian of the system. Because the basis functions are non-zero only within a given sector the corresponding matrices have a block diagonal structure. Each sector has an associated block which is coupled only to its nearest neighbors through the continuity conditions (Eq. 3.9). Note that the overlap matrix  $\underline{\Lambda}$ , whose elements are given by surface integrals over the basis functions[67], is particularly simple in the FEM representation. It contains only  $m_P$  non-zero elements (all equal to one). The integrals representing the matrix elements of  $\underline{\Gamma}$  are also particularly simple in the FEM representation. In fact, ex-

cept for the integral over the interaction potential, all can be done once and for all beforehand, significantly decreasing the cpu time necessary to construct the matrix. In addition, the  $\underline{\Gamma}$  matrix is symmetric which reduces the effort required to construct the matrix. The closed portion  $\underline{\Gamma}^{cc}$ , which is by far the largest matrix involved, can be written in banded format with dimensions  $(6m_{\max} - 1) \times (4m_{\max}n_{\max})$ , where the first term is the half-bandwidth. The actual storage required by LAPACK's banded format[63] is 3 times the half-bandwidth. The other large matrix required  $\underline{\Gamma}^{co}$  has dimensions  $(4m_{\max}n_{\max}) \times m_P$ . A general rule of thumb is to use at least four sectors per shortest wavelength in the problem which has achieved roughly 6 digits of accuracy in the phase shift, based on limited tests. The accuracy improves to  $\sim 8$  digits using 8 sectors/wavelength. Increasing the number of sectors is mainly a concern when memory becomes limited. For example, cpu time tests indicate that a single channel calculation using 1000 sectors requires less than 0.2 seconds on a DEC Alpha 400 MHz workstation. This number of sectors is generally adequate to describe most alkali two-body collisions. The cpu time scales roughly linearly with  $n_{\max}$  and quadratically with  $m_{\max}$ . Performance comparisons of this algorithm with a Numerov, Gordon, and integral equation[75] method are provided in Ref[76]. The FEM  $\underline{R}$ -matrix approach was found to be quite comparable to the integral equation method (another implicit approach) in speed, memory requirements, and accuracy. Both of these implicit approaches proved more accurate than the two explicit methods. No time comparisons were conducted with the Numerov and Gordon methods.

I use standard LAPACK[63] routines to solve equations 3.5 and 3.6. The eigenvalues  $b$  and eigenvectors  $\vec{c}^{\vec{d}}$  completely specify the linearly independent solutions of the Schrödinger equation on the surface  $\Sigma$ . This information is generally packaged in terms of a  $\underline{R}$ -matrix

$$R_{mm'} = - \sum_{\beta} Z_{m\beta} b_{\beta}^{-1} (Z^{-1})_{\beta m'} \quad (3.12)$$

where the columns of  $\underline{Z}$  are given by the eigenvectors  $\vec{c}^{\vec{d}}$ . Here  $\beta$  is the independent solution index.

### 3.1.3 Matching $\underline{R}$ -matrix boxes

The method outlined to this point assumes that equations 3.5 and 3.6 need to be solved only once to obtain an  $\underline{R}$ -matrix at sufficiently large  $R$  to apply the asymptotic boundary conditions. This is not always the case. Situations can arise which require either an unusually large number of sectors or many tens of channels to describe the collision process. This can result in a  $\Gamma^{cc}$  matrix which is too large to reside in memory. However, it is not necessary to abandon the FEM  $\underline{R}$ -matrix approach. One need only divide the radial domain into “boxes” and solve the  $\underline{R}$ -matrix equations **separately** in each box. The resulting solutions can be combined

in such a way that a final solution is obtained which is equivalent to solving the  $\underline{R}$ -matrix equations in a single box encompassing the entire radial domain and this is achieved with no loss of accuracy. This type of approach is sometimes called an “ $\underline{R}$ -matrix propagator” method[77].

A description of the matching procedure is simplified by considering the example shown in Fig. 3.1. The radial domain is divided into two boxes, A and B. Boundary conditions are specified on the inner boundary of box A ( $R = 0$ ) and left unspecified (i.e., left open) at  $R = R_I$ . In box B, the boundary conditions are left open at  $R = R_I$  and on the outer boundary  $R = R_{II}$ , except for channels which are strongly-closed at  $R_{II}$ . In these strongly-closed channels, we must impose boundary conditions to eliminate exponential growth. The resulting square solution matrix  $\underline{Z}$  has dimensions  $m_{\max} \times \beta_{\max}^A$  in A and  $(m_{\max} + m_P) \times \beta_{\max}^B$  in B, where  $m_{\max}$  is the total number of channels,  $m_P$  is the number of channels open or weakly-closed on  $R_{II}$ . For our particular example, the number of independent solutions in A is  $\beta_{\max}^A = m_{\max}$ , and  $\beta_{\max}^B = m_{\max} + m_P$  in box B. The first step is to require a linear combination of the independent solutions and their derivatives to be continuous across the boundary ( $R_I$ ) in each channel. This can be written as:

$$\begin{aligned} \sum_{\beta=1}^{\beta_{\max}^A} Z_{m\beta}^A D_{\beta}^A &= \sum_{\beta'=1}^{\beta_{\max}^B} Z_{m\beta'}^B D_{\beta'}^B \\ \sum_{\beta=1}^{\beta_{\max}^A} Z_{m\beta}^A b_{\beta}^A D_{\beta}^A &= - \sum_{\beta'=1}^{\beta_{\max}^B} Z_{m\beta'}^B b_{\beta'}^B D_{\beta'}^B \end{aligned} \quad (3.13)$$

where  $D$  represents the undetermined coefficients, the channel index  $m$  runs from  $1$ - $m_{\max}$  and the wave function derivatives have been written as  $Z'_{m\beta} = Z_{m\beta} b_{\beta}$ . The minus sign in the second condition comes from a reversal of the surface normal direction. As it stands, Eq. 3.13 is not sufficient to fully specify the coefficients  $D$ . A final condition is obtained by again requiring **constant** log derivatives on the outer boundary ( $R_{II}$ ). This requirement selects the  $\underline{R}$ -matrix eigenchannel solutions, which will be superimposed later to meet the physical boundary conditions relevant for either a scattering or photoabsorption process. This statement can be written as

$$\sum_{\beta'=1}^{\beta_{\max}^B} Z_{m'\beta'}^B b_{\beta'}^B D_{\beta'}^B = b_{\beta\ell} \sum_{\beta'=1}^{\beta_{\max}^B} Z_{m'\beta'}^B D_{\beta'}^B. \quad (3.14)$$

where now the channel index  $m'$  runs from  $m_{\max} + 1$  to  $m_{\max} + m_P$ . Equations 3.13 and 3.14 can be combined to form a generalized eigenvalue equation whose non-infinite eigenvalues determine the new log derivatives  $b_{\beta\ell}$  on the boundary  $R_{II}$ . The corresponding eigenvectors  $D$  give the new solution through expressions such

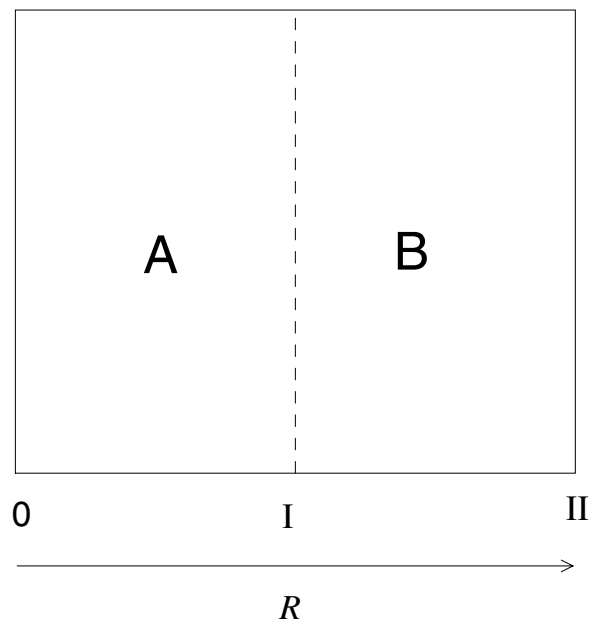


Figure 3.1: Division of the radial domain into two boxes A and B. The  $\underline{R}$ -matrix equations are solved separately from  $R = 0 \rightarrow R_I$  in A and from  $R_I \rightarrow R_{II}$  in B. Appropriate boundary conditions are applied at  $R = 0$  and  $R = R_{II}$ , leaving all channels open across  $R_I$ .

as:

$$Z_{m'\beta^f}^f = N_{\beta^f} \sum_{\beta'=1}^{\beta_{\max}^B} Z_{m'\beta'}^B D_{\beta'\beta^f}^B \quad (3.15)$$

where  $N_{\beta^f}$  is a normalization constant for each new independent solution. If it becomes necessary to divide the radial domain into many sectors this procedure can be iterated as many times as necessary to obtain the solution matrix and log derivatives on the final boundary.

### 3.2 Constructing the scattering matrix

At this stage, the  $\underline{R}$ -matrix represents mathematically correct solutions of the coupled Schrödinger equations. The physically relevant solutions are obtained by applying asymptotic boundary conditions (Eq. 2.5). At large  $R$ , where “large” is typically of the order  $10^3$  Bohr (occasionally  $10^5$  Bohr for systems that involve the long-range magnetic dipole interaction),  $V(R) \rightarrow \text{constant}$  and the two linearly independent solutions are the standard spherical Bessel  $j_l(k_m R)$  and Neumann  $n_l(k_m R)$  functions in each channel. A set of linearly-independent solutions at energy  $E$  can be written in this limit as[23]

$$\underline{M}(R) \xrightarrow{R \rightarrow \infty} \underline{f} - \underline{g} \underline{K} \quad (3.16)$$

where  $f_{mm'} = \sqrt{\frac{2\mu}{\pi k_m}} k_m R j_l(k_m R) \delta_{mm'}$  and  $g_{mm'} = \sqrt{\frac{2\mu}{\pi k_m}} k_m R n_l(k_m R) \delta_{mm'}$  are diagonal matrices of energy normalized spherical Bessel and Neumann functions. The real-valued constant reaction matrix  $\underline{K}$  determines the appropriate linear combination of  $f$  and  $g$ . It is evaluated by matching the log derivative of the wave function integrated from small  $R$  (Eq. 3.12) with the asymptotic form given in Eq. 3.16. The result written in terms of the  $\underline{R}$ -matrix is[23]

$$\underline{K} = [\underline{f} - \underline{f}' \underline{R}] [\underline{g} - \underline{g}' \underline{R}]^{-1} . \quad (3.17)$$

The  $\underline{S}$ -matrix, from which all physical observables can be evaluated, is related to the  $\underline{K}$ -matrix by the following[23]

$$\underline{S} = [\underline{1} + i\underline{K}] [\underline{1} - i\underline{K}]^{-1} \quad (3.18)$$

where  $i = \sqrt{-1}$ . Any scattering observable of interest can then be determined once this  $\underline{S}$ -matrix is constructed.

### 3.3 Adiabatic representation

Solving the diabatic two-body cold collision equations is the most straightforward approach for obtaining an  $\underline{S}$ -matrix. However, it does not always provide the most insight into the collision dynamics. Adiabaticizing the equations in  $R$  can be a useful step in this regard. A qualitative picture of the collision dynamics is obtained immediately from the adiabatic potentials and couplings. From a numerical standpoint, an  $\underline{S}$ -matrix obtained by solving the coupled adiabatic equations can be just as accurate as solution determined in a diabatic representation. However, in the two-body case it is actually more work to generate the adiabatic potentials and therefore this approach is presented mainly as a qualitative tool. This is not the case for the 3-body collisions presented in chapter 8, for which potentials and couplings have been calculated using the adiabatic hyperspherical method. An adiabatic variant of the FEM  $\underline{R}$ -matrix procedure has been developed to solve these equations and is outlined in Appendix B.

If we choose  $R$  as the adiabatic coordinate, the Hamiltonian can be separated into two terms  $H = T_R + H^{\text{ad}}$ , where the kinetic energy operator  $T_R$  contains all the derivative terms with respect to  $R$ . The adiabatic Hamiltonian  $H^{\text{ad}}$  is given by

$$H_{mm'}^{\text{ad}} = \delta_{mm'} \frac{l_m(l_m + 1)}{2\mu R^2} + V_{mm'} \quad (3.19)$$

where  $V_{mm'}$  includes the interaction potentials discussed in chapter 2.2 evaluated in an appropriate spin basis. Adiabatic eigenfunctions  $\Phi_\gamma$  and eigenvalues (adiabatic potentials)  $U_\gamma(R)$  of  $H^{\text{ad}}$  are calculated by parametric diagonalization of Eq. 3.19 as a function of  $R$ . The wave function can then be written in terms of the adiabatic eigenfunctions as [78, 79]

$$\Psi = \sum_{\gamma} \Phi_{\gamma}(\Omega, \chi; R) M_{\gamma}(R) , \quad (3.20)$$

where  $\Omega$  represents the angular degrees of freedom and  $\chi$  the spin degrees of freedom. Substituting this expansion back into the Hamiltonian gives the following representation for the coupled radial equations:

$$\left[ -\frac{1}{2\mu} \left( \frac{\partial}{\partial R} + \underline{P} \right)^2 + \underline{U} \right] \vec{M} = E \vec{M} . \quad (3.21)$$

All of the coupling (or nonadiabatic) effects are now contained in the real, antisym-

metric derivative coupling matrix  $\underline{P}(R)$  given by

$$P_{\gamma\gamma'} = \left\langle \Phi_{\gamma} \left| \frac{\partial}{\partial R} \Phi_{\gamma'} \right. \right\rangle . \quad (3.22)$$

The Born-Oppenheimer approximation neglects the  $\underline{P}$  matrix. I emphasize that the adiabatic formulation of the coupled Schrödinger equations is exact in principle, if  $\underline{P}$  is included and a complete angular momentum basis is used, which in the two-body case will always be possible in the Born-Oppenheimer limit[31], provided external magnetic fields can be neglected. Using a standard identity, Eq. 3.22 can be rewritten as

$$P_{\gamma\gamma'} = \begin{cases} \frac{\langle \Phi_{\gamma} | \partial H^{\text{ad}} / \partial R | \Phi_{\gamma'} \rangle}{U_{\gamma'} - U_{\gamma}} , & \gamma \neq \gamma' \\ 0, & \gamma = \gamma' \end{cases} . \quad (3.23)$$

For two-body collisions, evaluating the  $\underline{P}$  matrix is more straightforward with this approach since most of the terms in  $\underline{H}^{\text{ad}}$  are analytical functions of  $R$ . It is only necessary to take numerical derivatives of the small  $R$  part of the Born-Oppenheimer potentials.

As an example of the usefulness of this method, adiabatic potentials and derivative couplings are shown in Fig. 3.2 for the case of two  $^{87}\text{Rb}$  atoms colliding in an  $f=2$  total spin state. The two-body collision complex consists of three coupled channels (one singlet and two triplet Born-Oppenheimer potentials) with one channel converging to each of the three hyperfine split thresholds (see inset Fig. 2.1). Magnetic dipole couplings have been neglected so this represents a pure spin-exchange collision. The dynamics of spin-exchange collisions are extremely simple. The derivative couplings shown in Fig. 3.2.b indicate that transitions between spin channels occur almost exclusively in the neighborhood of  $R \sim 20 - 25$  a.u. This value of  $R$  is a fairly generic result for ground-state collisions in all the alkalis. The coupling region indicates the point at which exchange splitting in the Born-Oppenheimer potentials becomes comparable to the hyperfine splittings. Outside this transition region the wave functions in each channel evolve freely in the adiabatic potentials. At small  $R$  these potentials are basically the singlet or triplet Born-Oppenheimer potentials. Because the couplings are so localized and all channel crossings occur near the same  $R$ , the opportunity arises for the wave functions to interfere in such a way as to shut off spin-exchange losses. This is exactly the fortuitous situation with  $^{87}\text{Rb}$  collisions, which will be discussed in more detail in chapter 5.

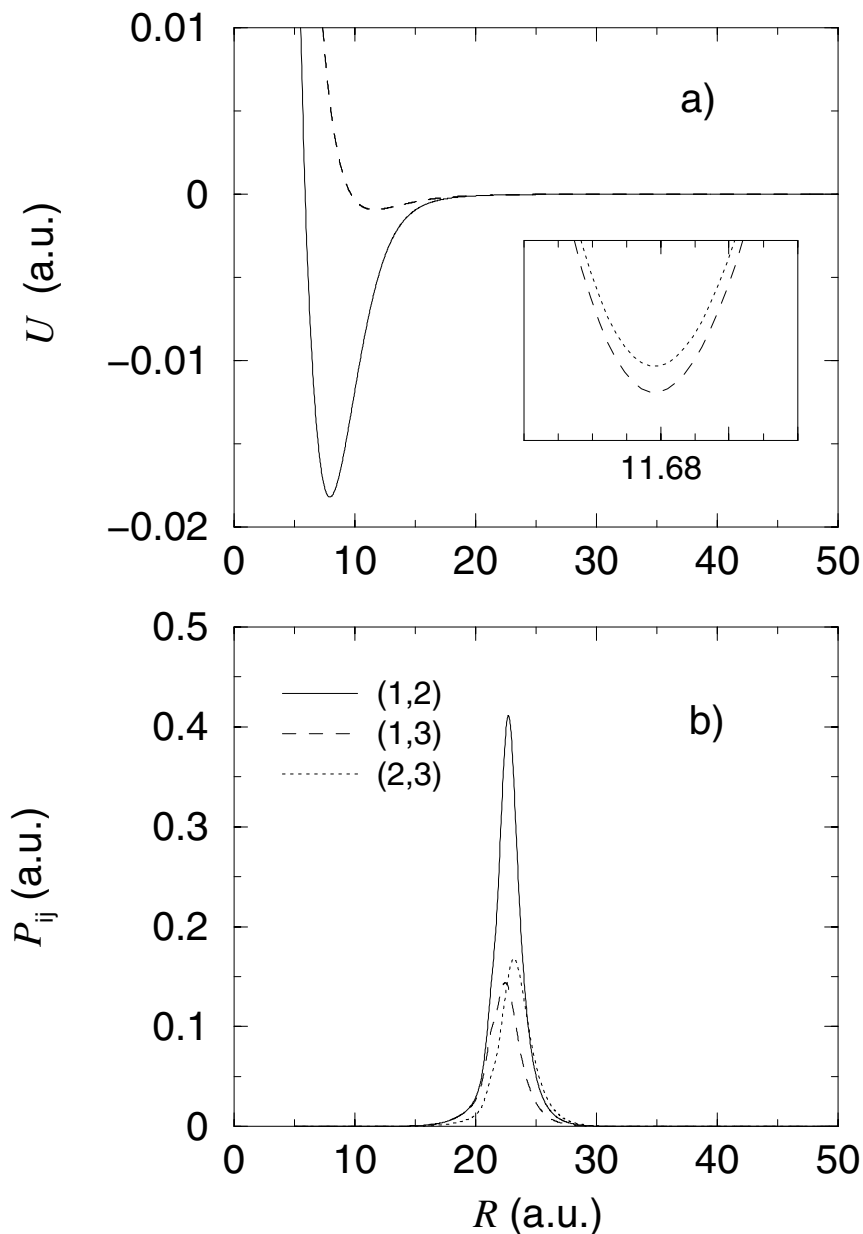


Figure 3.2: Adiabatic potentials a) and  $\underline{P}$ -matrix couplings b) for the  $s$ -wave collision of two  $^{87}\text{Rb}$  atoms in a  $f=2$  angular momentum state. The inset of a) shows the splitting of the two triplet-like potentials which is approximately equal to one hyperfine unit of energy ( $\Delta_{87} \simeq 10^{-6}$  a.u.). The adiabatic channel indices in b) are defined in order of increasing energy i.e., channel 1 is a singlet-like state converging to the 1+1 threshold. Channels 2 and 3 are predominately triplet states at small  $R$ , which correlate adiabatically to the 1+2 and 2+2 thresholds, respectively at  $R \rightarrow \infty$ .